Suspended GaN-based band-edge type photonic crystal nanobeam cavities

Tzeng Tsong Wu,[1] Hao Wen Chen,[1] Yu Pin Lan,[1] Tien Chang Lu,[1,*] and Shing Chung Wang[1]

[1]*Department of Photonics & Institute of Electro-Optical Engineering, National Chiao Tung University, Hsinchu 30050, Taiwan*
* timtclu@mail.nctu.edu.tw

Abstract: We demonstrated GaN-based photonic crystal (PC) nanobeam cavities by using the e-beam lithography and the suspended nanobeams were realized by focused-ion beam (FIB) milling. One resonant mode was clearly observed at 411.7 nm at 77K by optical pumping. The quality factor was measured to be to 7.4×10^2. Moreover, the degree of polarization value was measured to be 40%. The temperature-dependent characteristics were measured and discussed, which unambiguously demonstrated that the observed resonant peak originated from the band-edge mode of the one-dimensional PC nanobeam.

OCIS codes: (140.5960) Semiconductor lasers; (160.5298) Photonic crystals; (220.4241) Nanostructure fabrication.

References and links

1. E. Yablonovitch, "Inhibited spontaneous emission in solid-state physics and electronics," Phys. Rev. Lett. **58**(20), 2059–2062 (1987).
2. S. John, "Strong localization of photons in certain disordered dielectric superlattices," Phys. Rev. Lett. **58**(23), 2486–2489 (1987).
3. M. Meier, A. Mekis, A. Dodabalapur, A. Timko, R. E. Slusher, J. D. Joannopoulos, and O. Nalamasu, "Laser action from two-dimensional distributed feedback in photonic crystals," Appl. Phys. Lett. **74**(1), 7 (1999).
4. M. Imada, A. Chutinan, S. Noda, and M. Mochizuki, "Multidirectionally distributed feedback photonic crystal lasers," Phys. Rev. B **65**(19), 195306 (2002).
5. I. Vurgaftman and J. Meyer, "Design optimization for high-brightness surface-emitting photonic-crystal distributed-feedback lasers," IEEE J. Quantum Electron. **39**(6), 689–700 (2003).
6. H. Matsubara, S. Yoshimoto, H. Saito, Y. Jianglin, Y. Tanaka, and S. Noda, "GaN photonic-crystal surface-emitting laser at blue-violet wavelengths," Science **319**(5862), 445–447 (2008).
7. T. C. Lu, S. W. Chen, L. F. Lin, T. T. Kao, C. C. Kao, P. Yu, H. C. Kuo, S. C. Wang, and S. H. Fan, "GaN-based two-dimensional surface-emitting photonic crystal lasers with AlN/GaN distributed Bragg reflector," Appl. Phys. Lett. **92**(1), 011129 (2008).
8. S. Kawashima, T. Kawashima, Y. Nagatomo, Y. Hori, H. Iwase, T. Uchida, K. Hoshino, A. Numata, and M. Uchida, "GaN-based surface-emitting laser with two-dimensional photonic crystal acting as distributed-feedback grating and optical cladding," Appl. Phys. Lett. **97**(25), 251112 (2010).
9. M. Kim, C. S. Kim, W. W. Bewley, J. R. Lindle, C. L. Canedy, I. Vurgaftman, and J. R. Meyer, "Surface-emitting photonic-crystal distributed-feedback laser for the midinfrared," Appl. Phys. Lett. **88**(19), 191105 (2006).
10. O. Painter, R. K. Lee, A. Scherer, A. Yariv, J. D. O'Brien, P. D. Dapkus, and I. Kim, "Two-dimensional photonic band-Gap defect mode laser," Science **284**(5421), 1819–1821 (1999).
11. H. G. Park, S. H. Kim, S. H. Kwon, Y. G. Ju, J. K. Yang, J. H. Baek, S. B. Kim, and Y. H. Lee, "Electrically driven single-cell photonic crystal laser," Science **305**(5689), 1444–1447 (2004).
12. J. S. Foresi, P. R. Villeneuve, J. Ferrera, E. R. Thoen, G. Steinmeyer, S. Fan, J. D. Joannopoulos, L. C. Kimerling, H. I. Smith, and E. P. Ippen, "Photonic-bandgap microcavities in optical waveguides," Nature **390**(6656), 143–145 (1997).
13. M. Notomi, E. Kuramochi, and H. Taniyama, "Ultrahigh-Q nanocavity with 1D photonic gap," Opt. Express **16**(15), 11095–11102 (2008).
14. S. J. Kim, B. H. Ahn, J. Y. Kim, K. Y. Jeong, K. S. Kim, and Y. H. Lee, "Nanobeam photonic bandedge lasers," Opt. Express **19**(24), 24055–24060 (2011).
15. Y. Zhang, M. Khan, Y. Huang, J. Ryou, P. Deotare, R. Dupuis, and M. Lončar, "Photonic crystal nanobeam lasers," Appl. Phys. Lett. **97**(5), 051104 (2010).

16. R. Ohta, Y. Ota, M. Nomura, N. Kumagai, S. Ishida, S. Iwamoto, and Y. Arakawa, "Strong coupling between a photonic crystal nanobeam cavity and a single quantum dot," Appl. Phys. Lett. **98**(17), 173104 (2011).
17. I. S. Maksymov, "Optical switching and logic gates with hybrid plasmonic–photonic crystal nanobeam cavities," Phys. Lett. A **375**(5), 918–921 (2011).
18. Q. M. Quan, P. B. Deotare, and M. Lončar, "Photonic crystal nanobeam cavity strongly coupled to the feeding waveguide," Appl. Phys. Lett. **96**(20), 203102 (2010).
19. S. Kako, C. Santori, K. Hoshino, S. Götzinger, Y. Yamamoto, and Y. Arakawa, "A gallium nitride single-photon source operating at 200 K," Nat. Mater. **5**(11), 887–892 (2006).
20. T. C. Lu, J. R. Chen, S. C. Lin, S. W. Huang, S. C. Wang, and Y. Yamamoto, "Room temperature current injection polariton light emitting diode with a hybrid microcavity," Nano Lett. **11**(7), 2791–2795 (2011).
21. E. J. Cho and F. V. Bright, "Optical Sensor Array and Integrated Light Source," Anal. Chem. **73**(14), 3289–3293 (2001).
22. S. Sergent, M. Arita, S. Kako, S. Iwamoto, and Y. Arakawa, "High-Q (>5000) AlN nanobeam photonic crystal cavity embedding GaN quantum dots," Appl. Phys. Lett. **100**(12), 121103 (2012).
23. S. Sergent, M. Arita, S. Kako, K. Tanabe, S. Iwamoto, and Y. Arakawa, "High-Q AlN photonic crystal nanobeam cavities fabricated by layer transfer," Appl. Phys. Lett. **101**(10), 101106 (2012).
24. M. Arita, S. Ishida, S. Kako, S. Iwamoto, and Y. Arakawa, "AlN air-bridge photonic crystal nanocavities demonstrating high quality factor," Appl. Phys. Lett. **91**(5), 051106 (2007).
25. D. Neel, S. Sergent, M. Mexis, D. Sam-Giao, T. Guillet, C. Brimont, T. Bretagnon, F. Semond, B. Gayral, S. David, X. Checoury, and P. Boucaud, "AlN photonic crystal nanocavities realized by epitaxial conformal growth on nanopatterned silicon substrate," Appl. Phys. Lett. **98**(26), 261106 (2011).
26. N. V. Trivin, G. Rossbach, U. Dharanipathy, J. Levrat, A. Castiglia, J.-F. Carlin, K. A. Atlasov, R. Butt, R. Houdr, and N. Grandjean, "High quality factor two dimensional GaN photonic crystal cavity membranes grown on silicon substrate," Appl. Phys. Lett. **100**(7), 071103 (2012).
27. S. W. Chang, T. R. Lin, and S. L. Chuang, "Theory of plasmonic Fabry-Perot nanolasers," Opt. Express **18**(14), 15039–15053 (2010).
28. A. Tandaechanurat, S. Iwamoto, M. Nomura, N. Kumagai, and Y. Arakawa, "Increase of Q-factor in photonic crystal H1-defect nanocavities after closing of photonic bandgap with optimal slab thickness," Opt. Express **16**(1), 448–455 (2008).
29. J. R. Pugh, Y.-L. D. Ho, P. J. Heard, G. R. Nash, T. Ashley, J. G. Rarity, and M. J. Cryan, "Design and fabrication of a midinfrared photonic crystal defect cavity in indium antimonide," J. Opt. A, Pure Appl. Opt. **11**(5), 054006 (2009).
30. N. Okada, Y. Yamada, and K. Tadatomo, "Structural and optical evaluation of InGaN/GaN multi-quantum wells on template consisting of in-plane alternately arranged relaxed InGaN and GaN," J. Appl. Phys. **111**(4), 043508 (2012).
31. R. R. Reeber and K. Wang, "Lattice parameters and thermal expansion of GaN," J. Mater. Res. **15**(01), 40–44 (2000).
32. N. Watanabe, T. Kimoto, and J. Suda, "The temperature dependence of the refractive indices of GaN and AlN from room temperature up to 515 °C," J. Appl. Phys. **104**(10), 106101 (2008).

1. Introduction

Since photonic crystals (PCs) which can manipulate the light propagation direction and well confine photons were proposed in 1987, they have been widely investigated and applied in different optoelectronic devices such as lasers and light-emitting devices [1–3]. Basically, two kinds of PC lasers including band-edge and defect lasers have been studied and demonstrated [4–11]. For the PC band-edge lasers, the specific Bragg diffraction conditions were occurred at the photonic band-edge positions to achieve the laser threshold condition over a large lasing area. Meanwhile, the surface emitting condition can be met by specifically choosing the proper photonic band edges to form so-called photonic crystal surface emitting lasers [4–9]. As for the PC defect lasers with suspended membrane structures, the photonic band gap was created to confine photons in the defect cavity. The small mode volume (V) with a high quality (Q) factor can be observed in such kind of PC nanocavities [10, 11]. In recent years, PC nanobeam cavities, with further scaling the device footprints down but also maintaining the high Q factors, have attracted much attention and intensively researched [12–18]. Up to now, several reports of PC nanobeam cavities have been addressed such as PC nanobeam lasers with an ultralow threshold condition [15], observation of cavity quantum electrodynamics [16], optical switching devices [17] and photonic integrated circuits [18].

Usually, PC nanobeam cavities with suspended structures were realized in GaAs or InP-based material systems using selectively chemical etching [12–18]. In recent years, GaN and its ternary and quaternary alloys are very popular material system for novel optoelectronics

due to their large exciton binding energy (~26 meV) and wide range spectra tuning capability at the ultraviolet-visible region, which are attractive in the single photon emission [19] and strong coupling effect to tailor the exciton-polariton emission at room temperature [20] as well as the luminescence based bio-sensing application at the ultraviolet-visible region [21]. Very recently, defect type high Q AlN nanobeam PC cavities embedded with GaN quantum dots have been demonstrated using photo-electrochemical (PEC) etching [22, 23]. However, in GaN-based systems, the fabrication technologies of suspended structures are still challenging due to the specifically epitaxial structures and difficult etching process [24–26]. In this report, we demonstrated band-edge type GaN-based PC nanobeam cavities with suspended structures. The PC patterns and suspended nanobeam structures were fabricated by using the e-beam lithography and focused-ion beam (FIB). The plane wave expansion method (PWEM) [14] and finite element method (FEM) [27] were carried out to calculate the resonant wavelengths, quality factors and cavity heights of suspended GaN-based PC nanobeam cavities. Furthermore, the resonant mode of GaN-based PC nanobeam cavity was observed at 77K to 180K. Finally, the degree of polarization and temperature dependent micro-photoluminescence (μ-PL) properties of GaN-based PC nanobeam cavities were characterized and discussed.

2. Design and fabrication

Figure 1(a) shows the scheme of the suspended GaN-based PC nanobeam cavity. For designing the parameters of GaN-based PC nanobeam cavities, the corresponding band diagram was calculated by PWEM. Figure 1(b) shows the calculated band diagram of the GaN-based PC nanobeam cavities and solid lines represent the photonic bands. The first band (black curve) at the lowest frequency can be identified as the dielectric band and the other bands (blue and green curves) are the air-bands at higher frequency. On the other hand, when the in-plane wave vector k_x is close to band-edge positions, the group velocity of photons almost approached to zero. In this case, the Q factor of the cavities will increase and the photons will have higher probability to interact with the gain medium provided by InGaN/GaN multiple quantum wells (MQWs). Furthermore, the dielectric band is better for light-emitting devices due to good field overlapping with the gain medium [14]. Therefore the normalized frequency (a/λ, where a is the lattice period and λ is the wavelength) of our nanobeam was set to be around 0.44 locating at the center emission wavelength of the InGaN/GaN MQWs. However, the exact value of lattice period still depended on the nanobeam width (w), radius (r) of the PC hole and nanobeam cavity height (h).

It had been shown that the large nanobeam width would reduce the refractive index contrast between the dielectric medium and air hole and the small nanobeam width would result in higher scattering loss due to the more evanescent tail of the guided mode penetrating into the air [14]. To maintain a reasonable high quality factor of the nanobeam, the nanobeam width was determined to be 300 nm, corresponding to approximately 1.5a. Then, we used the finite element method (FEM) to calculate the Q factor depending on the r over a ratio (r/a) in order to select a proper radius of the PC air hole. Figure 2(c) shows the top view of the simulated electric field mapping in one unit cell. The modes we were monitoring were selected to be in the dielectric band as shown in the Fig. 2(c). The calculated Q factor versus the r/a ratio is shown in the Fig. 3(a). The different r/a ratio would influence the optical feedback mechanism in the nanobeam cavity. We observed that the best Q value was occurred when the r/a ratio was 0.25. Therefore, the parameters such as the radius, period of the PC and width of the nanobeam were selected to be 50, 200 and 300 nm, respectively.

Since that the width, period and the radius of the nanobeam were fixed, the cavity height was again optimized by using the FEM. The cavity heights from 1λ to 2.5λ were chosen to calculate the corresponding Q factor and confinement factor, respectively. Since the MQW region was embedded in the nanobeam cavity, the overlap ratio between the optical field and the MQW area had to be considered. Figure 1(d) shows the simulated electric field mapping

in one unit cell at z-x plane. The extracted transverse electric field along the z direction is also shown in the Fig. 1(d). Since the electric field distribution in the x-y plane was almost unchanged, the confinement factor was defined as the percentage of the squared electric field in the MQW region along the z direction. Figure 2(b) shows the calculated Q factor and optical confinement factor with respect to the cavity heights. The curves of quality factors and confinement factors showed different tendency. The Q factor would increase as the cavity height became larger, which is similar to the two dimensional PC slab for the first guided mode [28, 29]. However, when the cavity height became larger, the optical field would further stretch out of the MQW region and lower the confinement factor. With considering both the quality factor and the confinement factor, the optimized cavity height was between 1.5λ and 2λ. The calculated confinement factors of the cavity height 1.5λ and 2λ were similar. However, the quality factor of 2λ cavity height was higher than that of 1.5λ. Therefore, the cavity height was selected to be 2λ in our experiment which was around 320 nm.
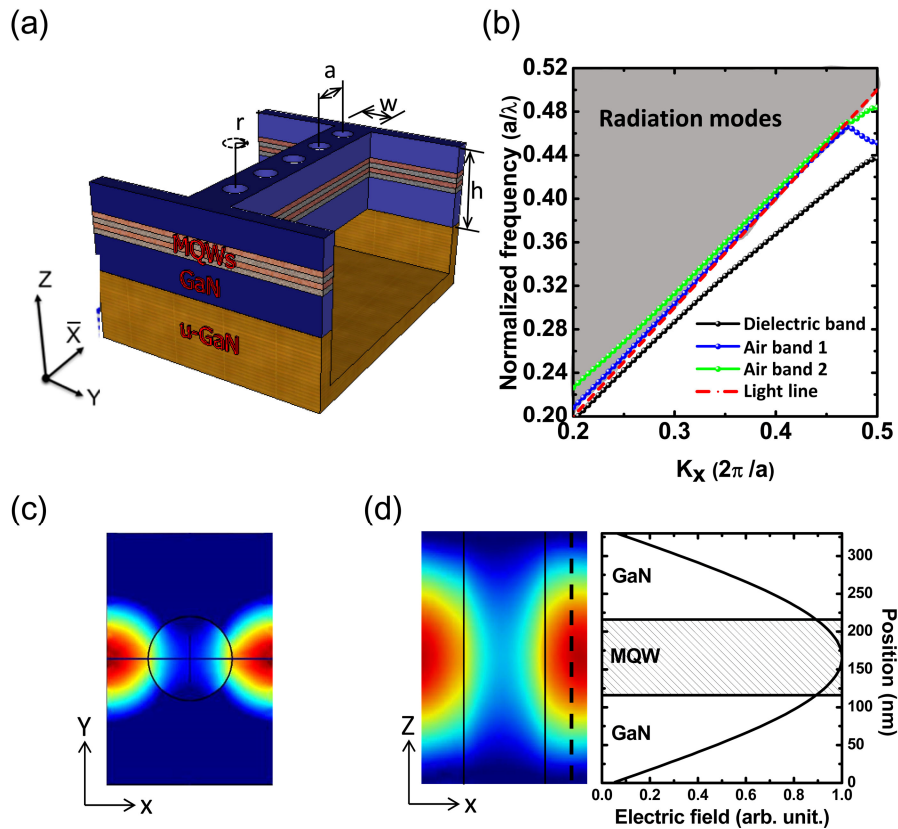

Fig. 1. (a) Scheme of the GaN-based PC nanobeam cavity, where w is the nanobeam width, h is the nanobeam cavity height, a is the lattice period, and r is the radius of one PC hole. The MQW region is sandwiched by two GaN layers with identical thickness. (b) The band diagram of GaN-based PC nanobeam cavity. The red dashed line represents the light line. The gray area above the light line represents the radiation modes. The black, blue and green curves represent the photonic bands with different guided modes. (c) Top view of the simulated electric field mapping in one unit cell. (d) Left: Cross sectional view of the simulated electric field mapping in one unit cell at the z-x plane. Right: Extracted electric field along the dash line in the left figure.

The suspended GaN-based PC nanobeam cavities were firstly grown on a c-plane 2-in sapphire substrate by the metal organic chemical vapor deposition system. The epitaxial structure consisted of a 2 μm-thick un-doped GaN layer, 10 pairs of InGaN/GaN MQWs, and

a 100 nm-thick un-doped GaN layer. The detailed growth parameters were similar to the previous report [7]. In the beginning, the hard mask 300 nm-thick SiN_x was deposited by the plasma enhanced chemical vapor deposition (PECVD). Then the 300 nm-thick poly-methyl methacrylate (PMMA) photoresist was coated by the spin coater. The one dimensional PC and nanobeam patterns were defined by e-beam lithography. Subsequently, the pattern was transferred to the SiN_x film by using reactive ion etching (RIE). Then the pattern on the hard mask was transferred to the GaN layer by using inductively coupled plasma (ICP). After that, the sample was cut and carefully polished from the wafer edge by chemical mechanical polishing (CMP) to form a flat plane quite close to the nanobeam pattern for preparing the undercut process to suspend the GaN thin film in the air. Finally, the underneath GaN layer was removed by FIB to accomplish the suspended nanobeam structures. The etching conditions of FIB had to be carefully controlled to prevent the distortion of the nanobeam cavity. Figures 2(c)-2(e) present the scanning electron microscope (SEM) images of the GaN-based PC nanobeam cavities. The PC nanobeam shape was carefully preserved and parameters including the period, radius, height and width were estimated to be 180 nm, 50 nm, 320 nm and 300 nm, respectively. A slightly upward protrusion of the PC nanobeam observed in Fig. 2(e) could be due to the partial compressive strain relaxation of the GaN and MQW layers suspended in the air. GaN-based PC nanobeam cavities were excited at 77K by a He-Cd 325 nm continuous wave laser. The laser beam with a spot size of about 7 μm was normally incident onto the devices. The μ-PL signal was collected by a 100X objective lens perpendicular to the devices surface or by a fiber with a 600 μm core in the normal plane of the sample. The collected signal was then fed into a spectrometer with a spectral resolution of approximately 0.07 nm.
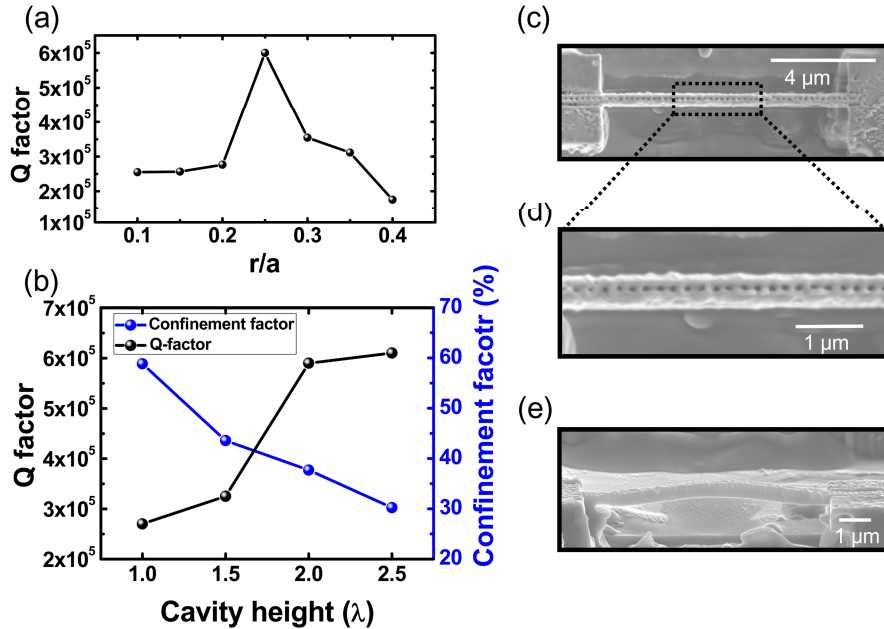

Fig. 2. (a) The calculated Q factor versus the r/a ratio. (b) The calculated Q factor and confinement factor versus the cavity height. The confinement factor was defined as the overlap ratio between the optical field and the MQW area as shown in Fig. 1(d) (c) The top view, (d) enlarged top view and (e) tilted angle view SEM images of the GaN-based PC nanobeam cavity. The parameters such as period and radius of PC were 180 nm and 50 nm. The height and width of nanobeam structure were 300 nm and 320 nm.

3. Results and discussion

The micro-PL (μ-PL) spectra of the as-grown planar sample with InGaN MQWs and the suspended GaN-based PC nanobeam cavity were shown in Figs. 3(a) and 3(b), respectively. The emission peak was around 407 nm in the planar sample with its full width at half maximum (FWHM) of about 10 nm. However, it can be found that there is only one resonant mode observed in the GaN-based PC nanobeam cavity. In order to further investigate the linewidth of this resonant mode, the Lorentzian peak function was used to fit the measured result, as shown in Fig. 3(b). The resonant wavelength was estimated to be 411.7 nm, corresponding to the normalized frequency of 0.438. It indicates that the resonant mode frequency was located at the dielectric band in the band diagram, matching to our design. In addition, the corresponding Q factor was calculated to be 7.4×10^2. Nevertheless, the Q factor in the experiment was much lower than that in the simulation which could be due to several factors: the protrusion of the PC nanobeam, finite length of the PC nanobeam, deviation of the r/a ratio, scattering loss and defect states caused by the imperfect fabrication process and the sidewall roughness of the GaN-based PC nanobeam cavity. Since the GaN epitaxial layer was grown on the sapphire substrate with large lattice mismatch, forming the PC nanobeam by removing the underneath GaN would release the compressive strain and deform the nanobeam itself. To mitigate this problem, the compressive strain could be relaxed first by inserting the superlattice or pre-strained layer before the MQW during the epitaxial growth [30].
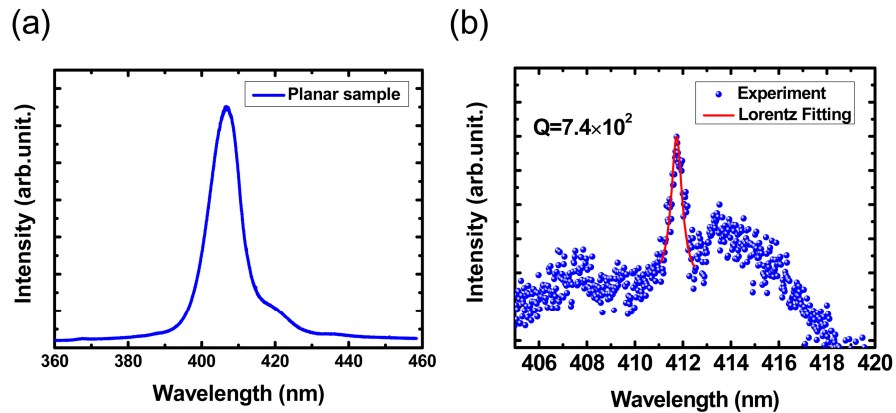
(a)   (b)

Fig. 3. The μ-PL spectra of (a) the planar sample and (b) the GaN-based 1D PC nanobeam cavity. The resonant wavelength and quality factor were calculated to be 411.7 nm and 742, respectively by using the Lorentz fitting in (b).

Figure 4(a) reveals the polarization characteristics of the GaN-based PC nanobeam cavity. The degree of polarization (DOP) is defined as $(I_{max}-I_{min})/(I_{max} + I_{min})$ where I_{max} and I_{min} are the maximum and the minimum intensity of the resonant mode peak. The polarization direction was y-polarized as defined in Fig. 1(a) which is similar to the band-edge type nanobeam lasers [14]. Besides, the degree of polarization (DOP) was measured to be 40%.

Figure 4(b) plots the evolution of μ-PL spectra from the GaN-based PC nanobeam cavity with increasing the temperature. One dominated mode can be clearly identified as the temperature was increased from 77K to 160K. However, the high Q resonant mode vanished while temperature was higher than 170K due to the increasing non-radiative recombination rate and absorption at higher temperature. Besides, it can be found that high-Q resonant mode showed the peak red-shift of 3.69 nm from 77K to 170K and the resonant mode peak red-shift rate was calculated to be 0.03 nm/K. It indicates that the peak position of resonant mode would be influenced by the temperature due to the refractive index variation and the nanobeam length variation. The nanobeam length variation could be estimated by the thermal

expansion coefficient of GaN [31] and the resonant mode peak red-shift rate was only in the order of 10^{-4} nm/K. On the other hand, based on the temperature dependent equation of the refractive index of GaN [32], the resonant mode peak position could be calculated by using the FEM and the peak shift value could be extracted to be 2.77 nm, which explained that the red-shift was resulted mainly from the variation of the refractive index. Moreover, the relatively larger mode peak red-shift rate observed in the experiment could be due to the worse heat dissipation causing larger index variation in the suspended PC nanobeam cavity.
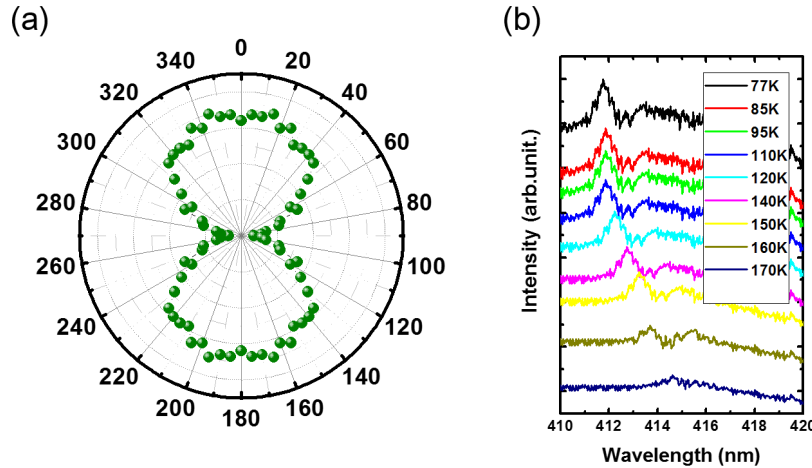

Fig. 4. (a) Polarization characteristics of the GaN-based 1D PC nanobeam cavity. The degree of polarization (DOP) was measured to be 40%. (b) Temperature-dependent μ-PL spectra of the GaN-based 1D PC nanobeam cavity. The red-shift rate of the resonant mode peak was calculated to be 0.03 nm/K.

4. Conclusion

In conclusion, suspended GaN-based PC nanobeam cavities were realized and characterized. The one dimensional PC pattern in a nanobeam was defined by e-beam lithography and the suspended nanobeam structure was realized by the FIB system. The resonant mode in the GaN-based PC nanobeam cavity was observed at 411.7 nm with a Q factor of 7.4×10^2 at 77K using the μ-PL measurement. Finally, the degree of polarization and the temperature-dependent characteristics of the GaN-based PC nanobeam cavity were measured and discussed. The DOP value was measured to be 40% and the peak red-shift rate was calculated to be 0.03 nm/K. By further optimized the structure parameters and fabrication conditions, the GaN-based nanobeam cavities with small footprint, high Q and temperature dependent characteristics could be promising for realization of room temperature single photon sources, extremely low threshold lasers and integration to the luminescence based bio-sensing application at the ultraviolet-visible region in the future.

Acknowledgments